LETTER

https://doi.org/10.1038/s41586-018-0091-5

Electron magnetic reconnection without ion coupling in Earth's turbulent magnetosheath

T. D. Phan[1]*, J. P. Eastwood[2], M. A. Shay[3], J. F. Drake[4], B. U. Ö. Sonnerup[5], M. Fujimoto[6], P. A. Cassak[7], M. Øieroset[1], J. L. Burch[8], R. B. Torbert[9], A. C. Rager[10,11], J. C. Dorelli[11], D. J. Gershman[11], C. Pollock[12], P. S. Pyakurel[3], C. C. Haggerty[3], Y. Khotyaintsev[13], B. Lavraud[14], Y. Saito[6], M. Oka[1], R. E. Ergun[15], A. Retino[16], O. Le Contel[16], M. R. Argall[9], B. L. Giles[11], T. E. Moore[11], F. D. Wilder[15], R. J. Strangeway[17], C. T. Russell[17], P. A. Lindqvist[18] & W. Magnes[19]

Magnetic reconnection in current sheets is a magnetic-to-particle energy conversion process that is fundamental to many space and laboratory plasma systems. In the standard model of reconnection, this process occurs in a minuscule electron-scale diffusion region[1,2]. On larger scales, ions couple to the newly reconnected magnetic-field lines and are ejected away from the diffusion region in the form of bi-directional ion jets at the ion Alfvén speed[3–5]. Much of the energy conversion occurs in spatially extended ion exhausts downstream of the diffusion region[6]. In turbulent plasmas, which contain a large number of small-scale current sheets, reconnection has long been suggested to have a major role in the dissipation of turbulent energy at kinetic scales[7–11]. However, evidence for reconnection plasma jetting in small-scale turbulent plasmas has so far been lacking. Here we report observations made in Earth's turbulent magnetosheath region (downstream of the bow shock) of an electron-scale current sheet in which diverging bi-directional super-ion-Alfvénic electron jets, parallel electric fields and enhanced magnetic-to-particle energy conversion were detected. Contrary to the standard model of reconnection, the thin reconnecting current sheet was not embedded in a wider ion-scale current layer and no ion jets were detected. Observations of this and other similar, but unidirectional, electron jet events without signatures of ion reconnection reveal a form of reconnection that can drive turbulent energy transfer and dissipation in electron-scale current sheets without ion coupling.

The magnetosheath region, which is located downstream of Earth's bow shock and consists of shocked solar wind, is highly turbulent. This region often contains hundreds of small-scale current sheets in which magnetic reconnection could potentially occur[9,10,12] (Fig. 1c). Many of these sheets are thin (ion inertial length scales or smaller), typically convecting past an observing spacecraft in a few seconds or less. If standard reconnection (Fig. 1a) were to operate in turbulent current sheets, then the ion jets in the extended exhausts should be the easiest reconnection signature to detect. Although electric-field and magnetic-field structures consistent with standard reconnection have been reported[9,10], in situ plasma measurements of the jets were not obtained for these thin current sheets because the data resolution using instruments on previous spacecraft (typically a few seconds per velocity measurement) was not sufficient to determine their presence or absence.

The four-spacecraft Magnetospheric Multiscale (MMS) mission, launched in 2015 and designed to reveal the kinetic physics of reconnection in near-Earth space, is flying in an electron-skin-depth-scale (about 7–10 km) tetrahedral formation. It measures three-dimensional electron and ion distributions at up to 7.5-ms and 37.5-ms resolution[13], respectively, which are 400 times and 80 times better resolved than previously available data. MMS observations of current sheets in the turbulent magnetosheath have revealed thin current sheets[14], fast electron flows[15,16] and electron heating[12,16]. These characteristics are similar to those observed in the electron-diffusion region of standard reconnection in large-scale current sheets at the outer edge of the magnetosphere (the magnetopause)[2,17] and in the laminar magnetosheath (which originate in the solar wind)[18,19]. However, ion jets, which should occur over a larger scale and therefore be more easily observed if standard reconnection is present in the current sheets in the turbulent magnetosheath, remain elusive. This raises the question of whether fast electron flows in these current sheets are produced by some process(es) besides reconnection.

Here we report the serendipitous simultaneous multi-spacecraft detection of oppositely directed super-ion-Alfvénic electron jets, parallel electric fields and magnetic-to-particle energy conversion in an electron-scale current sheet in the magnetosheath, providing direct evidence for reconnection without ion-scale coupling in turbulence.

In Fig. 2a–c we show the large-scale context of the MMS observations in the subsolar magnetosheath region on 2016 December 9 at 8:58–9:43 UT, with large fluctuations in both the magnitude of the magnetic field (Fig. 2a) and its components (Fig. 2b). Figure 2d–g reveals these fluctuations to be sharp changes in the magnetic field associated with large spikes in current density $\boldsymbol{j}$, many with $|\boldsymbol{j}| > 2\,\mu\mathrm{A\ m^{-2}}$ and comparable to the peak current densities observed in the electron-diffusion region at Earth's magnetopause[2,17,20]. Such large current densities across magnetic-field variations of a few tens of nanotesla imply current-sheet widths of a few tens of kilometres or less, less than the ion inertial length d_i of about 50 km in this interval. Closer inspection of the variations in current density and magnetic field throughout the interval in Fig. 2 reveals a range of current-sheet thicknesses: many, but not all, are of sub-ion scales.

To distinguish the regular fast electron flows associated with any thin current sheet from electron jets due to reconnection, data should be examined in a current-sheet ('LMN') coordinate system: the current-sheet normal points along $\boldsymbol{N}$, $\boldsymbol{L}$ is along the anti-parallel magnetic-field direction and $\boldsymbol{M} = \boldsymbol{N} \times \boldsymbol{L}$ is in the out-of-plane ('X-line') direction (Fig. 1a). In such a frame, the main current is in the M direction, while the bi-directional reconnection outflows are in the $\pm L$ directions (Fig. 1b). Definitive evidence for reconnection would be the simultaneous detection of oppositely directed plasma outflow jets by two spacecraft located on opposite sides of the X-line[4].

Such an event was captured at around 09:03:54 UT, when $|\boldsymbol{j}|$ reached approximately $3\,\mu\mathrm{A\ m^{-2}}$ (red arrow in Fig. 2g). In Fig. 3 we show this current sheet in detail, which had a magnetic shear of 14° (the guide

[1]Space Sciences Laboratory, University of California, Berkeley, CA, USA. [2]The Blackett Laboratory, Imperial College London, London, UK. [3]University of Delaware, Newark, DE, USA. [4]University of Maryland, College Park, MD, USA. [5]Dartmouth College, Hanover, NH, USA. [6]ISAS/JAXA, Sagamihara, Japan. [7]West Virginia University, Morgantown, WV, USA. [8]Southwest Research Institute, San Antonio, TX, USA. [9]University of New Hampshire, Durham, NH, USA. [10]Catholic University of America, Washington, DC, USA. [11]NASA Goddard Space Flight Center, Greenbelt, MD, USA. [12]Denali Scientific, Healy, AK, USA. [13]Swedish Institute of Space Physics, Uppsala, Sweden. [14]Institut de Recherche en Astrophysique et Planétologie, Université de Toulouse, Toulouse, France. [15]University of Colorado LASP, Boulder, CO, USA. [16]CNRS/Ecole Polytechnique, Paris, France. [17]University of California, Los Angeles, Los Angeles, CA, USA. [18]Royal Institute of Technology, Stockholm, Sweden. [19]Space Research Institute, Austrian Academy of Sciences, Graz, Austria. *e-mail: phan@ssl.berkeley.edu

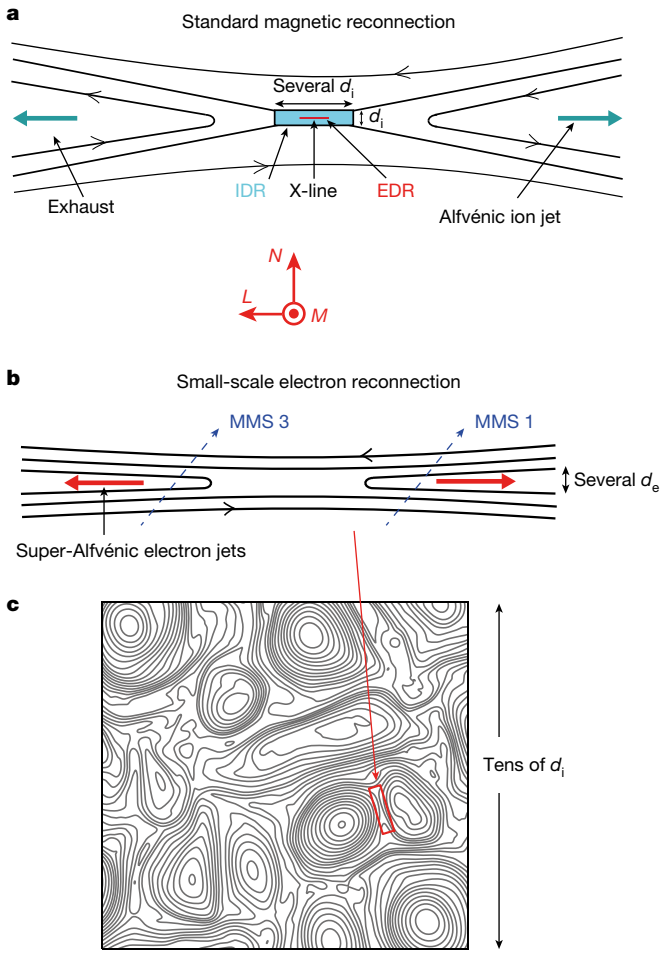

Fig. 1 | Schematics contrasting standard magnetic reconnection in large-scale current sheets and electron-only reconnection in small-scale turbulence. The reconnection configurations in **a** and **b** are displayed in the current-sheet (LMN) coordinate system. **a**, In standard reconnection, the magnetic topology changes in the small electron-diffusion region (EDR) around the X-line, but most of the magnetic-to-particle energy conversion happens in the extended exhausts, with bi-directional ion jetting and heating. The width of the electron-diffusion region (along N) is of the order of the electron skin depth d_e, whereas its length along $\pm L$ could be up to an ion inertial length, $d_i = 43d_e$. The electron-diffusion region is embedded in an ion-diffusion region (IDR), whereas the magnetohydrodynamic-scale reconnection exhaust can extend thousands of d_i (along L) away from the X-line[5]. **b**, Schematic of reconnection in an electron-scale current sheet involving only electrons, with no ion coupling. The entire current sheet is essentially the electron-diffusion region, having a single (electron) scale with embedded bi-directional super-ion-Alfvénic jets. MMS 1 and MMS 3 trajectories through the current sheet relative to the X-line are overlaid (dashed arrows), deduced on the basis of the directions of the electron jets observed on 2016 December 9 at around 09:03:54 UT (and shown in Fig. 3). MMS 1 and MMS 3 were on opposite sides of the X-line detecting bi-directional electron jets. The slanted spacecraft trajectories take into account the likely motion (in the spacecraft frame) of the X-line due to the presence of an external electron flow along $+L$ of about 150 km s^{-1}. **c**, Schematic showing the formation of multiple small (d_i-scale) magnetic structures and thin (d_e-scale) current sheets at their interfaces in turbulent plasmas, informed by turbulence simulations[8,12].

field was $B_M \approx 40$ nT, compared to an anti-parallel field of $|B_L| \approx 5$ nT). Four-spacecraft timing analysis finds the thickness of the current sheet to be only 4 km (or 4 electron skin depths, d_e), determined from the crossing duration of 45 ms (between the vertical dashed lines in Fig. 3) and the convection speed of $V_N = 95$ km s^{-1} of the current sheet.

Inside this electron-scale current sheet, both MMS 3 (left) and MMS 1 (right) observed fast out-of-plane electron flows ($V_{eM} \approx 900$ km s^{-1}; Fig. 3c, m) that produced the main current j_M (Fig. 3d, n) and the associated reversal of B_L (Fig. 3a, k). The speed V_{eM} is comparable to the inflow electron-Alfvén speed of $V_{AeL} = 1{,}000$ km s^{-1} based on $B_L \approx 5$ nT and an electron number density of 20 per cubic centimetre.

Coincident with the intense current layers, MMS 3 and MMS 1 simultaneously observed oppositely directed electron jets in the outflow (L) direction, with $\Delta V_{eL} \approx +250$ km s^{-1} at MMS 3 (Fig. 3c) and $\Delta V_{eL} \approx -450$ km s^{-1} at MMS 1 (Fig. 3m), relative to an external electron flow in the L direction of $V_{eL} \approx +150$ km s^{-1}. The speeds of these electron outflow jets were roughly 10–18 times the asymptotic ion-Alfvén speed (based on B_L) of $V_{AiL} \approx 25$ km s^{-1}. As expected for a reconnection geometry with inflow from both sides, the changes in B_L for MMS 1 are correlated with those in V_{eL} in the first part of the field change and anti-correlated in the second half, whereas for MMS 3 the reverse holds. An exception to this behaviour is that MMS 3, but not MMS 1, observed an electron jet with $\Delta V_{eL} \approx -300$ km s^{-1} at the right edge of the current sheet that is opposite to the main ΔV_{eL} jet (Fig. 3c). Simulations of standard reconnection with a strong guide field have shown such ΔV_{eL} edge jet[21]. The lack of a reversed jet at the edge of the current sheet at MMS 1 is currently not understood.

The measurements of oppositely directed electron outflow jets at MMS 1 and MMS 3 are further supported by the higher-resolution (0.125 ms) measurements of the L component of the field-line velocity $\boldsymbol{E} \times \boldsymbol{B}/B^2$ (where $\boldsymbol{E}$ is the electric field and $\boldsymbol{B}$ is the magnetic field), which was negative at MMS 1 and positive at MMS 3 (except for a negative dip at the right edge, similar to that in V_{eL}) (Fig. 3q, g). These $(\boldsymbol{E} \times \boldsymbol{B}/B^2)_L$ outflows were predominantly perpendicular to the magnetic field, owing to the large B_M (Fig. 3a, k); E_N (Fig. 3e, o), which is opposite at the two spacecraft, together with the dominant B_M, drives the outflows. Crucially, MMS 3 was located 7.1 km in the $+L$ direction relative to MMS 1 so that the observations are consistent with diverging jets from a reconnection X-line located between the two spacecraft as they pass through the reconnecting current sheet. There was no evidence for ion jets (ΔV_{iL}) at the ion-Alfvén speed (Fig. 3b, l) within the thin current sheet. That ion jets are absent is not surprising, because the thickness of the current sheet was only $0.09d_i$ (or 0.08 ion gyroradius) and the observations were made within $7d_e$ of the X-line.

What is surprising, however, is that the electron-scale reconnecting current sheet was not embedded inside a much larger ion-scale current sheet, as would be expected (and observed) in standard reconnection[1,18–20,22] (Fig. 1a). The absence of an outer ion-scale current sheet can be seen in Fig. 3a, k (see also Extended Data Fig. 1), which shows B_L reaching its asymptotic values immediately outside the thin current sheet.

Both spacecraft detected well defined parallel electric fields (Fig. 3f, p), which implies that the 'electron frozen-in condition' ($\boldsymbol{E}' = \boldsymbol{E} + \boldsymbol{V}_e \times \boldsymbol{B} = \boldsymbol{0}$) was violated. Furthermore, $\boldsymbol{j} \cdot \boldsymbol{E}'$ was positive (Fig. 3j, t) and dominated by $j_{\parallel}E_{\parallel}$, indicating non-ideal magnetic-to-particle energy conversion[23] characteristic of the electron-diffusion region. However, unlike for standard reconnection, where most of the magnetic energy is converted into ion jetting and heating, here, half of the available magnetic energy per particle (half of 6 eV) in the inflow regions ($m_e(V_{AeL})^2$, where m_e is the electron mass) goes into kinetic energy associated with ΔV_{eM} and ΔV_{eL}, which are 90% and 45% of V_{AeL}, respectively. The remaining half (3 eV), if converted entirely into electron heating, would lead to an increase in electron temperature of (3 eV) $\times$ $(\gamma-1)/\gamma \approx 1$ eV in the reconnecting current sheet[24], where $\gamma = 5/3$ is the ratio of specific heats. Such a small temperature increase would not be discernible in the data (Fig. 3i, s).

Within the 21-min burst data intervals shown in Fig. 2a, there were 34 other isolated current sheets with $|\boldsymbol{j}| > 2\,\mu$A m^{-2}, which implies sub-ion-scale current-sheet widths. Surprisingly, the majority of these current sheets had low magnetic shears (that is, strong guide fields): 23 of the 34 events had magnetic shear of less than 45°. All 34 sheets had a fast out-of-plane electron velocity V_{eM} consistent with the large current density j_M, but only 16 displayed clear super-ion-Alfvénic V_{eL} jets that could be related to reconnection. In each of these cases, all four spacecraft detected V_{eL} pointing in the same direction and were

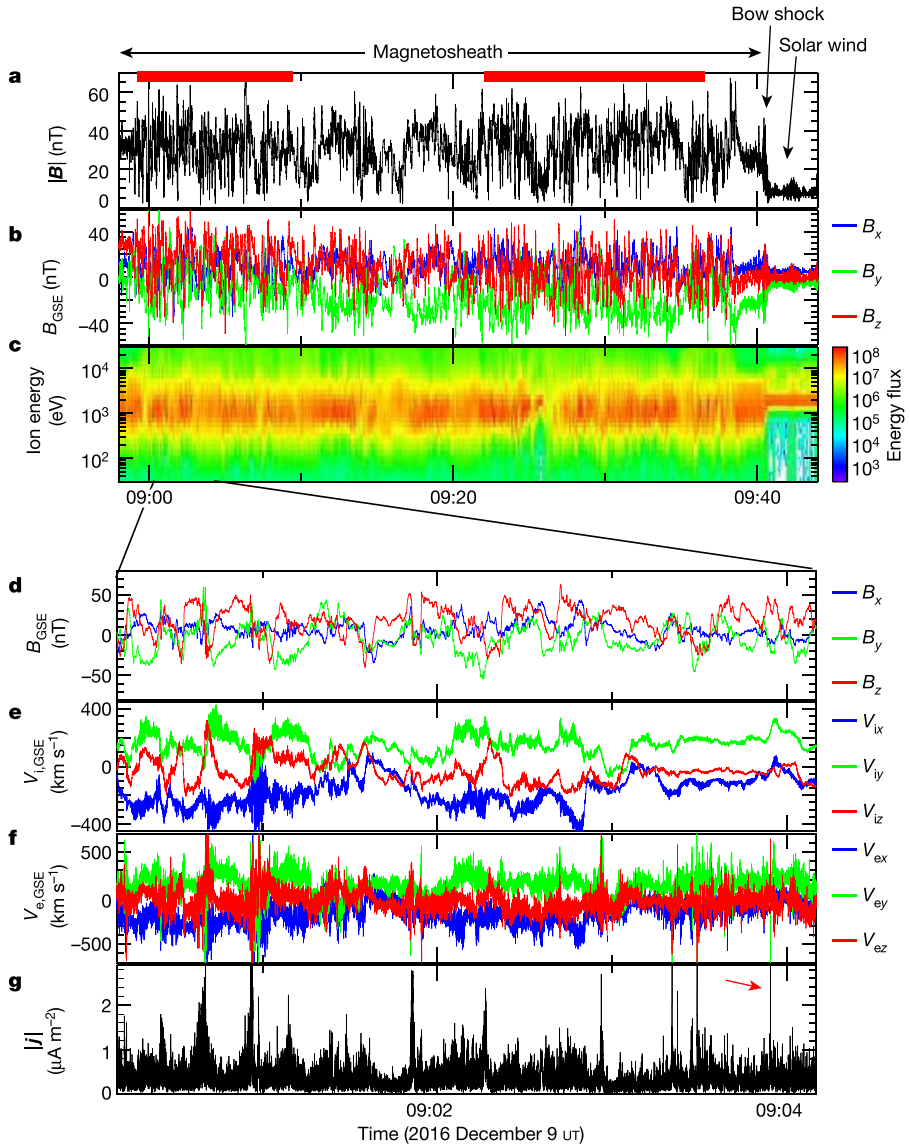

Fig. 2 | Overview of MMS 1 observations of turbulent current sheets in Earth's subsolar magnetosheath region downstream of a quasi-parallel shock. The observations reveal the presence of large spikes in current density (more than 2 μA m^{-2}), which imply sub-ion-scale current sheets. The data are displayed in the geocentric solar ecliptic (GSE) coordinates. **a**, **b**, The magnitude (**a**; $|B|$) and components (**b**; B_x, B_y and B_z) of the magnetic field. c, The ion energy–time spectrogram of differential energy flux (colour scale, in units of eV s^{-1} cm^{-2} sr^{-1} eV^{-1}). **d**–**g**, Zoomed-in (4-min) interval showing the magnetic field (**d**; B_x, B_y and B_z), ion velocity (**e**; V_{ix}, V_{iy} and V_{iz}), electron velocity (**f**; V_{ex}, V_{ey} and V_{ez}) and current density (**g**; $|\boldsymbol{j}| = \boldsymbol{j} = eN_e(V_i - V_e)$, where e is the elementary charge and N_e is the electron number density) computed from plasma measurements. Throughout the interval in **a**–**c**, the angle between the magnetic field of the solar wind and the Sun–Earth line was less than 30° and the subsolar bow shock was quasi-parallel. The spike in current density at around 09:03:54 UT (indicated by the red arrow in **g**) is the bi-directional electron jet event, shown in detail in Fig. 3. Red horizontal bars in **a** denote burst data intervals totalling 21 min, selected by the MMS scientist on duty because they contained a large number of high-amplitude magnetic-field fluctuations (with $\Delta B/B \approx 0.5$), suggestive of current sheets that could be prone to reconnection.

therefore embedded in the same jet. The scarcity of unambiguous reconnection events with divergent jets (which implies that the X-line is located between the spacecraft) is probably due to the small (about 7 km or $7d_e$) separations between the spacecraft.

We found no evidence for reconnection ion jetting associated with any of the electron outflow jet events, or in any other (including ion-scale-thick) current sheets in the 21-min interval (see examples in Extended Data Fig. 2). This finding is in stark contrast to standard models of reconnection in which the ion exhaust jets should be easier to detect than the electron-diffusion region because they extend large distances from the X-line.

The absence of ion reconnection signatures suggests that, in these turbulent magnetosheath plasmas, there is insufficient space and/or time for the ions to couple to the magnetic structures. This could occur not only because the widths of the current sheets are of electron scales, but also if the overall dimensions of the current sheets are limited because ion coupling requires some minimum lengths along the exhaust[25] (L) and X-line[26] (M) directions. A hybrid simulation study of resistive reconnection with no guide field[25] suggests that ions become decoupled when the length of the current sheet in the L direction (Fig. 1c) falls below about $10d_i$. If such an ion decoupling scale also exists in strong-guide-field collisionless reconnection, although potentially at a smaller scale than $10d_i$, then it could account for our observed lack of ion coupling in reconnection in the magnetosheath, in which the coherence scales of magnetic structures have been reported[27] to be of the order of d_i.

The experimental discovery of electron-only reconnection reveals that reconnection operates differently in current sheets with small

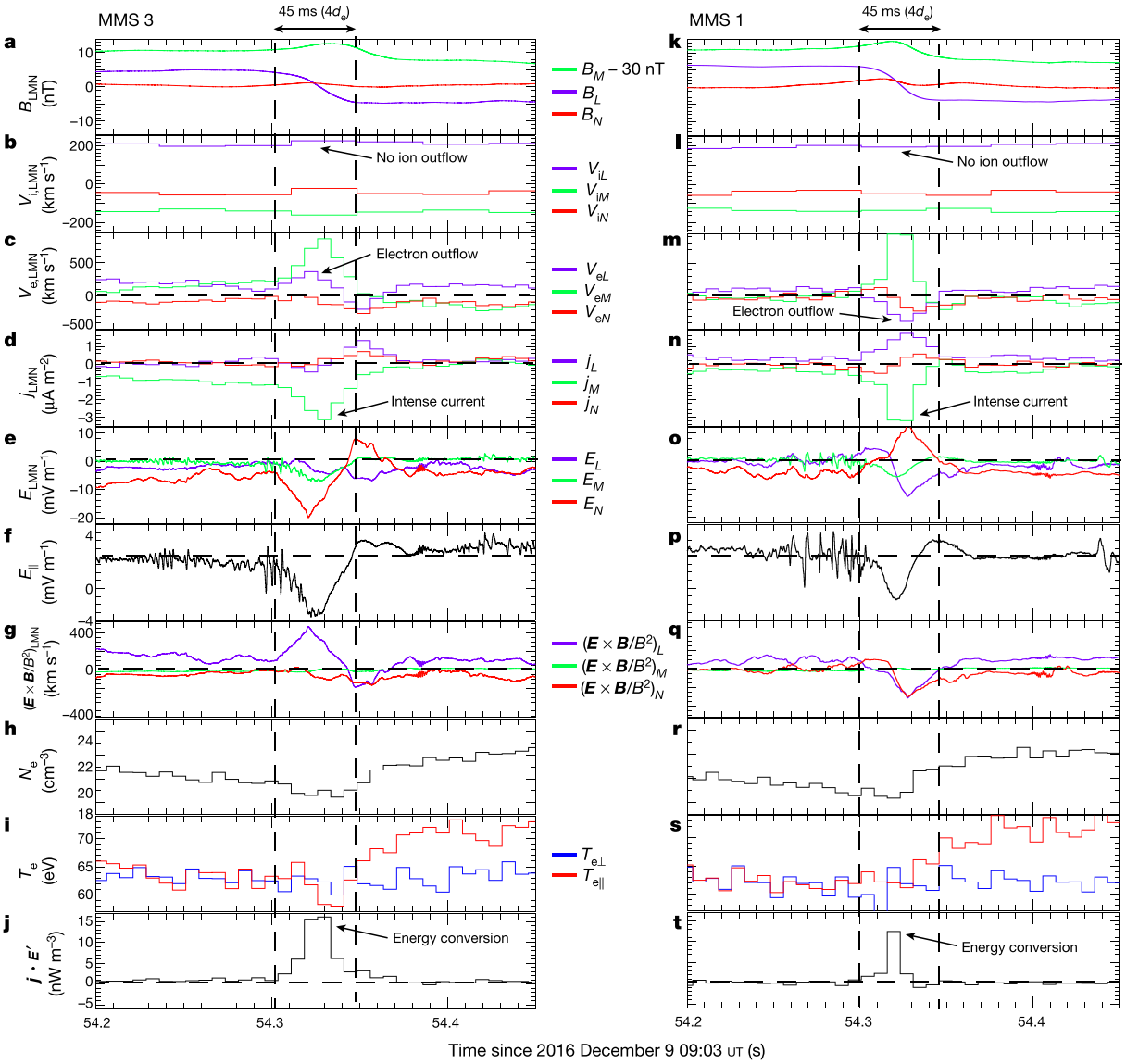

Fig. 3 | Simultaneous MMS 1 and MMS 3 detections of oppositely directed super-ion-Alfvénic electron jets, parallel electric fields and enhanced magnetic-to-electron energy conversion in an electron-scale current sheet. The data for both spacecraft (MMS 3, **a**–**j**; MMS 1, **k**–**t**) are shown in a common current-sheet (LMN) coordinate system, determined for the MMS 3 crossing of the current sheet at 09:03:54.270–09:03:54.365 UT, with $\boldsymbol{L} = (-0.091, 0.87, 0.49)_{GSE}$, $\boldsymbol{M} = (-0.25, -0.49, 0.83)_{GSE}$ and $\boldsymbol{N} = (0.96, -0.05, 0.27)_{GSE}$. The vertical dashed lines mark the left and right edges of the current sheet. **a**, **k**, Magnetic field B_{LMN} at 8,196 samples per second (from merged fluxgate and search-coil magnetometer measurements[28]), with B_M shifted by −30 nT. **b**, **c**, **l**, **m**, Ion (**b**, **l**; $V_{i,LMN}$) and electron (**c**, **m**; $V_{e,LMN}$) velocity. The 7.5-ms electron and 37.5-ms ion data products were generated by separating the individual energy sweeps that were used to form the nominal burst-mode distribution functions. These data maintain sufficient angular coverage to recover accurate plasma moments at four times the nominal temporal resolution[13]. **d**, **n**, Current density (j_{LMN}) from plasma measurements. **e**, **o**, Electric field[28] in the spacecraft frame (E_{LMN}) at 8,196 samples per second. **f**, **p**, Electric-field component parallel to the magnetic field ($E_{||}$). **g**, **q**, $(\boldsymbol{E} \times \boldsymbol{B}/B^2)_{LMN}$ velocity. **h**, Electron density (N_e). **i**, Electron temperature (T_e). **j**, **t**, $\boldsymbol{j} \cdot (\boldsymbol{E} + \boldsymbol{V}_e \times \boldsymbol{B}) = \boldsymbol{j} \cdot \boldsymbol{E}'$. The LMN coordinate system was determined using a hybrid minimum-variance method, which often works best in low-magnetic-shear current sheets[29]. The current-sheet normal direction N was determined from $\boldsymbol{B}_1 \times \boldsymbol{B}_2/|\boldsymbol{B}_1 \times \boldsymbol{B}_2|$, where $\boldsymbol{B}_1$ and $\boldsymbol{B}_2$ are the fields at the two edges of the current sheet. We define $\boldsymbol{M} = \boldsymbol{L}' \times \boldsymbol{N}$, where $\boldsymbol{L}'$ is the direction of maximum variance of the magnetic field[30]; $\boldsymbol{L} = \boldsymbol{N} \times \boldsymbol{M}$. MMS 3 was located at $L = +7.1$ km, $M = +3.3$ km and $N = +1.6$ km relative to MMS 1. Data from all four spacecraft are shown in Extended Data Fig. 3.

overall dimensions. Our finding supports the long-held idea that reconnection has a role in dissipating the energy associated with plasma turbulence in space and astrophysical systems, although the scale for dissipation by reconnection would be at the electron scale instead of the ion scale. To assess the importance of reconnection in dissipating turbulence energy in small systems quantitatively, the basic properties of electron-only reconnection (such as the rate, duration and onset conditions of reconnection) will need to be investigated theoretically and observationally. These properties could differ substantially from those known from the standard model of reconnection.

Data availability

The entire MMS dataset is publicly available at https://lasp.colorado.edu/mms/sdc/public/.

Online content

Any Methods, including any statements of data availability and Nature Research reporting summaries, along with any additional references and Source Data files, are available in the online version of the paper at https://doi.org/10.1038/s41586-018-0091-5.

Received: 7 December 2017; Accepted: 30 January 2018;
Published online 9 May 2018.

1. Vasyliunas, V. M. Theoretical models of magnetic merging. *Rev. Geophys.* **13**, 303–336 (1975).
2. Burch, J. L. et al. Electron-scale measurements of magnetic reconnection in space. *Science* **352**, aaf2939 (2016).
3. Paschmann, G. et al. Plasma acceleration at the Earth's magnetopause: evidence for reconnection. *Nature* **282**, 243–246 (1979).
4. Phan, T. D. et al. Extended magnetic reconnection at the Earth's magnetopause from detection of bi-directional jets. *Nature* **404**, 848–850 (2000).
5. Gosling, J. T., Skoug, R. M., McComas, D. J. & Smith, C. W. Direct evidence for magnetic reconnection in the solar wind near 1 AU. *J. Geophys. Res.* **110**, A01107 (2005).
6. Petschek, H. E. Magnetic field annihilation. In Proc. AAS-NASA Symposium on the Physics of Solar Flares (ed. Hess, W. N.) 425–439 (NASA, 1964)
7. Matthaeus, W. H. & Lamkin, S. L. Turbulent magnetic reconnection. *Phys. Fluids* **29**, 2513–2534 (1986).
8. Servidio, S., Matthaeus, W. H., Shay, M. A., Cassak, P. A. & Dmitruk, P. Magnetic reconnection in two-dimensional magnetohydrodynamic turbulence. *Phys. Rev. Lett.* **102**, 115003 (2009).
9. Retinò, A. et al. In situ evidence of magnetic reconnection in turbulent plasma. *Nat. Phys.* **3**, 235–238 (2007).
10. Sundqvist, D., Retinò, A., Vaivads, A. & Bale, S. D. Dissipation in turbulent plasma due to reconnection in thin current sheets. *Phys. Rev. Lett.* **99**, 025004 (2007).
11. Haggerty, C. C. et al. Exploring the statistics of magnetic reconnection X-points in kinetic particle-in-cell turbulence. *Phys. Plasmas* **24**, 102308 (2017).
12. Chasapis, A. et al. Electron heating at kinetic scales in magnetosheath turbulence. *Astrophys. J.* **836**, 247 (2017).
13. Rager, A. C. et al. Electron crescent distributions as a manifestation of diamagnetic drift in an electron scale current sheet: magnetospheric multiscale observations using new 7.5 ms fast plasma investigation moments. *Geophys. Res. Lett.* **45**, 578–584 (2018).
14. Eriksson, E. et al. Strong current sheet at a magnetosheath jet: kinetic structure and electron acceleration. *J. Geophys. Res.* **121**, 9608–9618 (2016).
15. Yordanova, E. et al. Electron scale structures and magnetic reconnection signatures in the turbulent magnetosheath. *Geophys. Res. Lett.* **43**, 5969–5978 (2016).
16. Vörös, Z. et al. MMS observations of magnetic reconnection in the turbulent magnetosheath. *J. Geophys. Res.* **122**, 11442–11467 (2017).
17. Chen, L. J. et al. Electron energization and mixing observed by MMS in the vicinity of an electron diffusion region during magnetopause reconnection. *Geophys. Res. Lett.* **43**, 6036–6043 (2016).
18. Phan, T. D., Drake, J. F., Shay, M. A., Mozer, F. S. & Eastwood, J. P. Evidence for an elongated (60 ion skin depths) electron diffusion region during fast magnetic reconnection. *Phys. Rev. Lett.* **99**, 255002 (2007).
19. Wilder, F. D. et al. Multipoint measurements of the electron jet of symmetric magnetic reconnection with a moderate guide field. *Phys. Res. Lett.* **118**, 265101 (2017).
20. Burch, J. L. & Phan, T. D. Magnetic reconnection at the dayside magnetopause: advances with MMS. *Geophys. Res. Lett.* **43**, 8327–8338 (2016).
21. Pritchett, P. L. Geospace environment modeling magnetic reconnection challenge: simulations with a full particle electromagnetic code. *J. Geophys. Res.* **106**, 3783–3798 (2001).
22. Shay, M. A. et al. Structure of the dissipation region during collisionless magnetic reconnection. *J. Geophys. Res.* **103**, 9165–9176 (1998).
23. Zenitani, S., Hesse, M., Klimas, A. & Kuznetsova, M. New measure of the dissipation region in collisionless magnetic reconnection. *Phys. Rev. Lett.* **106**, 195003 (2011).
24. Shay, M. A. et al. Electron heating during magnetic reconnection: a simulation scaling study. *Phys. Plasmas* **21**, 122902 (2014).
25. Mandt, M. E. et al. Transition to whistler mediated magnetic reconnection. *Geophys. Res. Lett.* **21**, 73–76 (1994).
26. Meyer, J. C. *Structure of the Diffusion Region in Three Dimensional Magnetic Reconnection*. PhD thesis, Univ. Delaware (2015).
27. He, J. S. et al. Two-dimensional correlation functions for density and magnetic field fluctuations in magnetosheath turbulence measured by the Cluster spacecraft. *J. Geophys. Res.* **116**, A06207 (2011).
28. Torbert, R. B. et al. The FIELDS instrument suite on MMS: scientific objectives, measurements, and data products. *Space Sci. Rev.* **199**, 105–135 (2016).
29. Gosling, J. T. & Phan, T. D. Magnetic reconnection in the solar wind at current sheets associated with extremely small field shear angles. *Astrophys. J.* **763**, L39 (2013).
30. Sonnerup, B. U. Ö. & Cahill, L. J. Jr. Magnetopause structure and attitude from Explorer 12 observations. *J. Geophys. Res.* **72**, 171–183 (1967).

Acknowledgements We are grateful for the dedicated efforts of the MMS team. We thank J. Gosling, who inspired us to search for unconventional reconnection in space. This work was supported by NASA contract number NNG04EB99C at SwRI, which funded work at most of the co-authors' institutions in the United States. The work at U. C. Berkeley was supported by NASA grants 80NSSC18K0157 and NNX08AO83G. UK involvement at Imperial College was supported by STFC (UK) grant ST/N000692/1. The French involvement (SCM instruments) on MMS is supported by CNES, CNRS-INSIS and CNRS-INSU.

Reviewer information *Nature* thanks G. Paschmann and the other anonymous reviewer(s) for their contribution to the peer review of this work.

Author contributions T.D.P. carried out the data analysis, interpretation and manuscript preparation. J.P.E., M.A.S., J.F.D., B.U.Ö.S., M.F., P.A.C., M.Ø., P.S.P., C.C.H., M.O., and A.R. contributed to the data interpretation and manuscript preparation. J.L.B. led the successful design and operation of the MMS mission and contributed to the interpretation of the data. A.C.R., J.C.D., D.J.G., C.P., B.L., B.L.G., T.E.M., and Y.S. contributed to the development and operation of and the interpretation of data from the Fast Plasma instruments. R.B.T., R.E.E., Y.K., M.R.A., F.D.W. and P.A.L. contributed to the development and operation of and the interpretation of data from the electric-field experiments. O.L.C. contributed to the development and operation of the search-coil magnetometers. C.T.R., R.J.S., and W.M. contributed to the development and operation of the fluxgate magnetometers.

Competing interests The authors declare no competing interests.

Additional information

Extended data is available for this paper at https://doi.org/10.1038/s41586-018-0091-5.

Correspondence and requests for materials should be addressed to T.D.P.

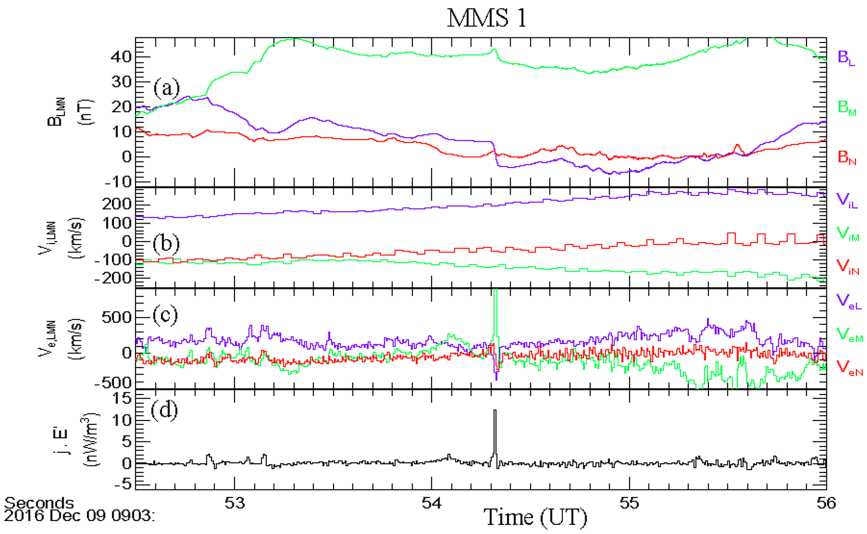

Extended Data Fig. 1 | Large-scale context of the thin current sheet, illustrating the fact that the electron-scale current sheet was a stand-alone current sheet, not embedded inside an ion-scale one. Data are shown in the LMN coordinates determined for the thin current sheet and used in Fig. 3. **a**, Magnetic field. **b**, Ion velocity. **c**, Electron velocity. **d**, $\boldsymbol{j}\cdot(\boldsymbol{E}+\boldsymbol{V}_e\times\boldsymbol{B})=\boldsymbol{j}\cdot\boldsymbol{E}'$. The thin reconnecting current sheet stands out in this interval, with nothing else approaching its current density or its value of $\boldsymbol{j}\cdot(\boldsymbol{E}+\boldsymbol{V}_e\times\boldsymbol{B})$. The absence of an ion-scale current sheet enveloping the electron-scale current sheet is indicated by the fact that $|B_L|$ reaches essentially its asymptotic values immediately outside the thin current sheet.

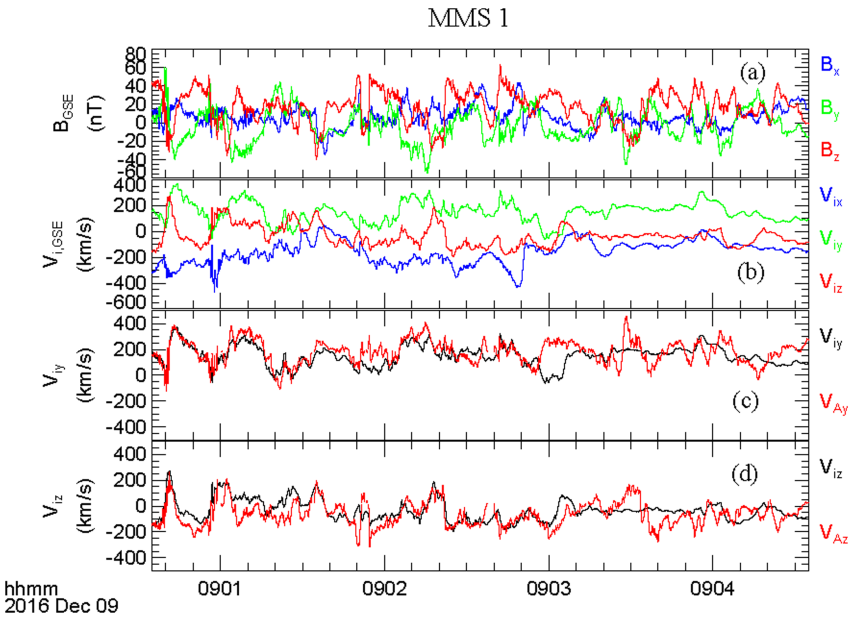

Extended Data Fig. 2 | Absence of reconnection ion jetting. The data are in GSE coordinates. **a**, Magnetic field. **b**, Ion velocity. **c**, **d**, y (**c**) and z (**d**) components of the ion velocity ($\boldsymbol{V}_i$) and Alfvén velocity ($\boldsymbol{V}_A$). $\boldsymbol{V}_A$ is relative to the reference velocity, density and magnetic-field values at the left edge of the data interval: $\boldsymbol{V}_A = \boldsymbol{B}_{ref}(1-\alpha_{ref})^{1/2}(\mu_0\rho_{ref})^{-1/2} - \boldsymbol{B}(1-\alpha)^{1/2}(\mu_0\rho)^{-1/2}$, where μ_0 is the vacuum permeability, $\alpha = (p_{||}-p_\perp)\mu_0/B^2$ is the pressure anisotropy factor and ρ is the mass density of the plasma[3]. The expected speeds of the ion reconnection jets embedded inside many of the large-magnetic-shear current sheets are in the range of 100–200 km s^{-1}, based on B_L variations of around 20−40 nT (**a**). If present, such jets are readily recognized by back-to-back opposite correlations between ion velocity and magnetic-field variation at the two edges of the current sheet, which indicate pairs of rotational discontinuities emanating from the X-line[5]. These signatures are not seen here. What we instead find in the data is either no correlation between components of $\boldsymbol{V}_i$ and $\boldsymbol{B}$, or a single correlation (or anti-correlation), indicative of Alfvénic structures[16] rather than reconnection jetting.

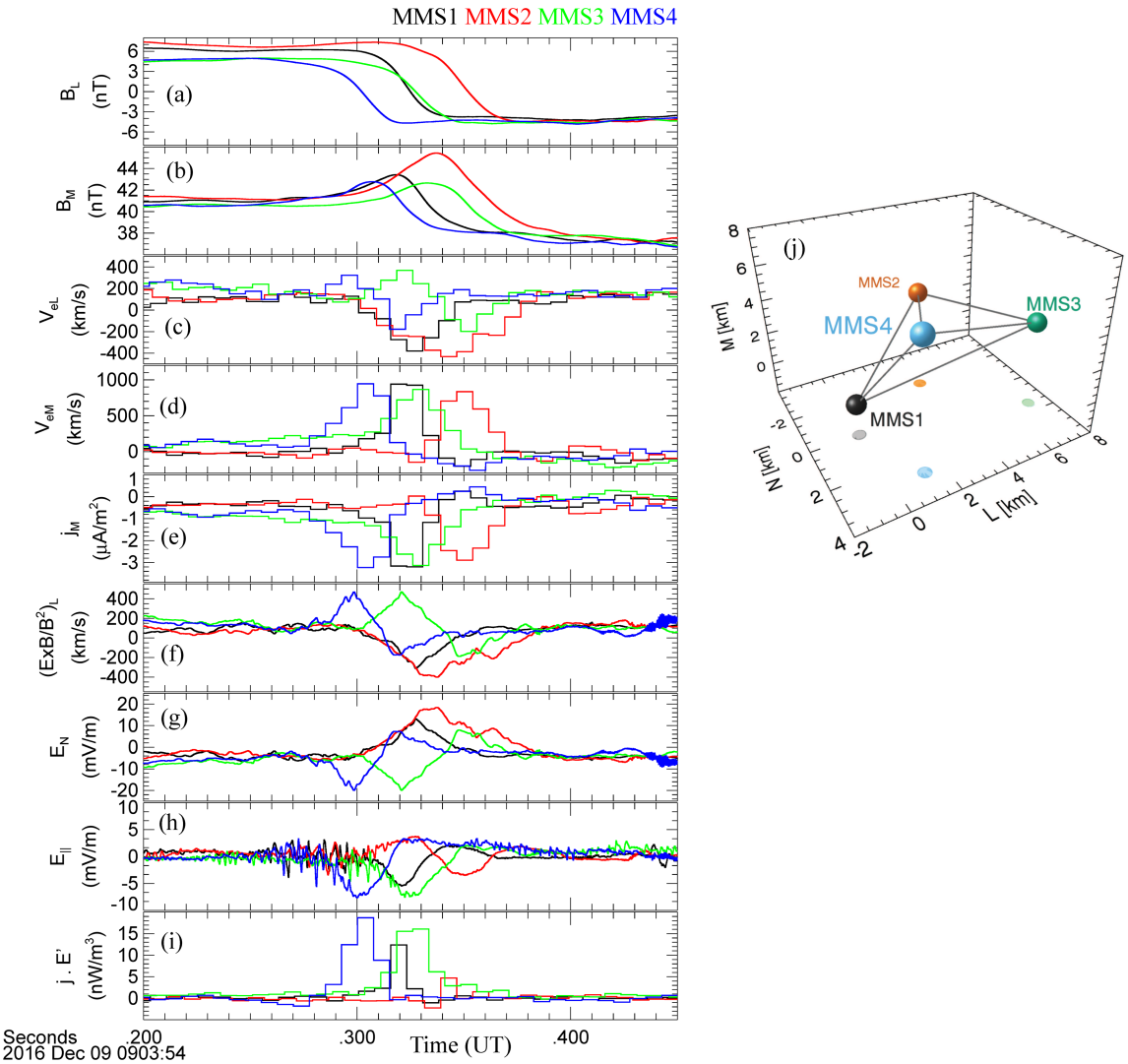

Extended Data Fig. 3 | Four-spacecraft observations of the reconnecting current sheet. A common current-sheet LMN coordinate system (same as in Fig. 3) was used for consistency, justified by the fact that the LMN coordinates at individual spacecraft differ from each other by less than 4°. **a**–**d**, L (**a**, **c**) and M (**b**, **d**) components of the magnetic field (**a**, **b**) and of the electron velocity (**c**, **d**). **e**, M component of the current density. **f**, L component of the $\boldsymbol{E}\times\boldsymbol{B}/B^2$ velocity. **g**, N component of the electric field. **h**, Electric-field component parallel to the magnetic field. **i**, $\boldsymbol{j}\cdot(\boldsymbol{E}+\boldsymbol{V}_e\times\boldsymbol{B})=\boldsymbol{j}\cdot\boldsymbol{E}'$. **j**, Spacecraft locations relative to MMS 1, in kilometres (roughly d_e). The B_L profiles (**a**) show that MMS 1 and MMS 3 crossed the current sheet at essentially the same time, preceded by MMS 4 and followed by MMS 2. The fact that MMS 4 exited the current sheet before MMS 2 entered it places an upper limit on the thickness of the current sheet, which is the 4.5-km separation distance between the two spacecraft along $\boldsymbol{N}$ (**j**). This is consistent with the current-sheet width of 4 km determined from the motion and crossing duration of the current sheet. Inside the current sheet, MMS 4 detected a positive $(\boldsymbol{E}\times\boldsymbol{B}/B^2)_L$ (except at the right edge), similarly to MMS 3, whereas MMS 2 detected a negative $(\boldsymbol{E}\times\boldsymbol{B}/B^2)_L$, similarly to MMS 1. This indicates that there was a pair of spacecraft on each side of the X-line. All four spacecraft detected a predominantly negative $E_{||}$. The parameter $\boldsymbol{j}\cdot(\boldsymbol{E}+\boldsymbol{V}_e\times\boldsymbol{B})$ was consistently positive at all four spacecraft throughout the current sheet, with the amplitude being lowest at MMS 2. MMS 2 also detected the largest guide-field (B_M) compression, fastest ΔV_{eL} and $(\boldsymbol{E}\times\boldsymbol{B}/B^2)_L$ jets, slowest ΔV_{eM} and weakest $E_{||}$, which together may suggest that MMS 2 was furthest away from the X-line.